Annals of Nuclear Energy 195 (2024) 110183

Contents lists available at ScienceDirect

Annals of Nuclear Energy

journal homepage: www.elsevier.com/locate/anucene

Coded-Aperture imaging based on random code and Backpropagation neural network

Zeyu Wang [a,b,1], Chao Wang [a,1], Pin Gong [a,b,*], Liansheng Li [c,*], Zhimeng Hu [a,d], Yongqiang Shi [c], Xiaolei Shen [a], Cheng Zhou [e], Xiaoxiang Zhu [e], Xiaobin Tang [a,d]

[a] Department of Nuclear Science and Technology, Nanjing University of Aeronautics and Astronautics, Nanjing 210016, China
[b] State Key Laboratory of Intense Pulsed Radiation Simulation and Effect, Xi'an 710024, China
[c] Beijing Institute of Control Engineering, Beijing 100094, China
[d] Key Laboratory of Nuclear Technology Application and Radiation Protection in Astronautics, Ministry of Industry and Information Technology, Nanjing 210016, China
[e] Jiangsu Nuclear and Radiation Safety Supervision and Management Center, Nanjing 210019, China

ARTICLE INFO

Keywords:
Coded-aperture imaging
BPNN
Random code
Monte Carlo simulation

ABSTRACT

Coded-aperture radiation imaging technology has important application value in the field of space radiation detection. A coded-aperture imaging algorithm based on random code and Backpropagation neural network (BPNN) is proposed for high quality imaging of x-rays and gamma rays in space environments. The experimental results show that BPNN can improve the signal-to-noise ratio of the reconstructed image when applied to the reconstruction process of coded-aperture imaging based on random code. Therefore, it has a good application prospect in the field of space coded-aperture imaging.

1. Introduction

Observations of cosmic hard X-rays and gamma rays (10–500 keV) can provide us with direct information about some high-energy phenomena (~ 10^{20} eV) in the universe (Phillips et al., 2008). However, gamma-ray bursts are fast and transient, with low photon flux reaching the detector and strong environmental background. This requires imaging equipment to quickly and accurately locate the direction of gamma-ray bursts in a complex radiation environment. Coded-aperture imaging technology uses a multi-aperture collimator with a preset pattern to modulate the cosmic rays and reconstructs the data detected by the array detector to obtain the direction of the source (Cenker-amaddi et al., 2012; Ding et al., 2016). It has the advantages of excellent detection efficiency and high reconstruction contrast-to-noise ratio (CNR).

The coding sequences of coded-aperture imaging generally have random array, uniformly redundant array (URA) (Shen et al., 2020; Macwilliams and Sloane, 1977) and modified uniformly redundant array (MURA) (Cieślak et al., 2016) and other arrays. Compared with coding arrays, such as URA and MURA, the random array is not limited by mathematical rules, and has good design flexibility. It can set the size and select the opening rate as required (Fenimore and Cannon, 1978; Gottesman and Fenimore, 1989). Thus, the random array can be flexibly designed according to the task objective during the application process makes the coding function flexibly designed according to the task objectives during the application process. However, When X-rays or gamma rays from multiple directions pass through the random coded collimator, the background noise generated by rays in each direction is superimposed, which results in a high background and poor contrast in the image. Therefore, it is a crucial research topic to improve the imaging quality of coded-aperture imaging based on random code.

Coded-aperture imaging method based on random array was originally decoded using correlation methods and iterative decoding algorithm (Gottesman and Fenimore, 1989; Martineau et al., 2010). The correlation analysis method has the advantage of remarkable time-saving. However, it can only be used to rehabilitate the coding features of the image, and the noise from many aspects cannot be effectively suppressed (Cieślak et al., 2016). The MLEM method uses a large number of iterative calculations to obtain high-quality reconstructed images (Ballesteros et al., 2001; Berrim et al., 1996). However, the reconstruction speed of this algorithm will decrease significantly when the detector array is large.

The latest coded-aperture imaging decoding method proposed by our research group is artificial neural network, which is widely used in the

* Corresponding authors.
[1] These authors contributed equally to this work.

https://doi.org/10.1016/j.anucene.2023.110183
Received 21 June 2022; Received in revised form 2 October 2023; Accepted 9 October 2023

field of nuclear technology, such as energy spectrum analysis and nuclide recognition (Olmos et al., 1992; He et al., 2018). The MURA collimator was successfully decoded by the Convolutional Neural Network (CNN) method (Zhang et al., 2019) and a clear reconstructed image was obtained. This method can reconstruct the image of the radioactive source quickly and accurately, which can be used for real-time measurement and dynamic monitoring of cosmic hard X-rays and gamma rays.

In this study, the BPNN method is used to decode the random encoding, which overcomes the inherent high background of the random encoding to improve the CNR and improve the speed of image reconstruction. In the Particle and Heavy Ion Transmission Code System (PHITS) (Sihver et al., 2007), an imaging device based on cadmium zinc telluride (CZT) pixel detector and random coding was built to simulate the imaging process of X-rays and gamma rays to complete the BPNN training. The experimental device is set up, verifying the performance of the method, and the BPNN reconstruction is compared with related analysis methods.

2. Principle

The birth of random array is the most direct method to solve the low detection efficiency of pinhole imaging, the idea is that the probability and position of openings in the generated encoding function are random. The correlation analysis method obtains the theoretically optimal reconstructed image by selecting the coding array whose correlation is similar to the delta function (Fenimore and Cannon, 1978), which has the advantage of remarkable time-saving. In the actual imaging process, the background noise comes from the transmission and scattering of photons with different energy, device processing and assembly errors, near-field effect and amplification effect to a certain extent, and detector electronic noise. For example, the noise of CdZnTe pixel array detection system mainly comes from the incomplete charge collection noise, the equivalent electronic noise of readout circuit, and the leakage current noise of crystal surface electrode. The radioactive source image is reconstructed by the decoding method of correlation operation. When performing the periodic autocorrelation operation, the coding matrix and the decoding matrix have the highest peak value when they completely coincide. Because the coding method is random, when performing the correlation operation on the decoding matrix shift, the opening units of the coding matrix and the decoding matrix may overlap, resulting in uneven background sidelobe in the reconstructed image, also known as inherent noise. Fig. 1 lists the autocorrelation function of a 16 × 16 random coding array and the cyclic autocorrelation function of a one-dimensional random sequence with a length of 256. It can be seen that in addition to the peak, the background noise is superimposed with the inherent noise, and this noise cannot be artificially removed during reconstruction. In this paper, a new reconstruction method based on BPNN was proposed to obtain reconstructed images under random array conditions.

BPNN has arbitrarily complex pattern classification ability and excellent multi-dimensional function mapping ability, which makes them perform well in image reconstruction and object recognition (He et al., 2018). A BPNN consists of input layer, hidden layer, and output layer. In each training of BPNN, the loss function is calculated by comparing the output value obtained by the neural network with the target output value, and the error is fed back layer by layer through the BP algorithm, until the error between the output value of the neural network and the current output value is within an acceptable range. Therefore, the hidden layer may be used to reduce the effects of noise in the coded image to obtain reconstructed images with decreased noise.

3. Methods

The reconstruction process(Fig. 2) based on BPNN is mainly divided into four steps:

1. Design a mask of random array to model the geometric relationship between the radioactive source, the mask and the detector in the Particle and Heavy Ion Transport Code System (PHITS).
2. The radioactive source imaging process is simulated using the Monte Carlo method and then coded images are divided into train set and test set.
3. Construct the BPNN network, train the network with the training set, and test the network with the simulated test set.
4. The coded images obtained by the experimental device are used for the experimental test set, and CNR is used to evaluate the quality of reconstructed image and the reconstruction capability of the BPNN-based method.

3.1. Monte Carlo model construction

The training data were obtained by Monte Carlo simulation, and the image model was constructed using the PHITS program. The CZT detector is widely used for X-ray and gamma-ray imaging due to its high energy and spatial resolution. The size of the CZT detector (McCleskey et al., 2015; Grindlay et al., 2011) used was 25.5 × 25.5 × 5 mm^3, divided into 16 × 16 pixels, with a single pixel size of 1.5 mm × 1.5 mm × 5 mm. The coded-aperture imaging telescope usually need to continuously monitor a large area for a long time to deal with unknown direction information due to the random occurrence of high-energy radiation events in the entire sky in space. At the same time, it needs imaging in orbit in a short time; thus, the detection satellite can accurately observe the X-rays and gamma rays in the follow-up (Fitzgerald et al., 2013; Krimm et al., 2013). Under this premise, random coding and

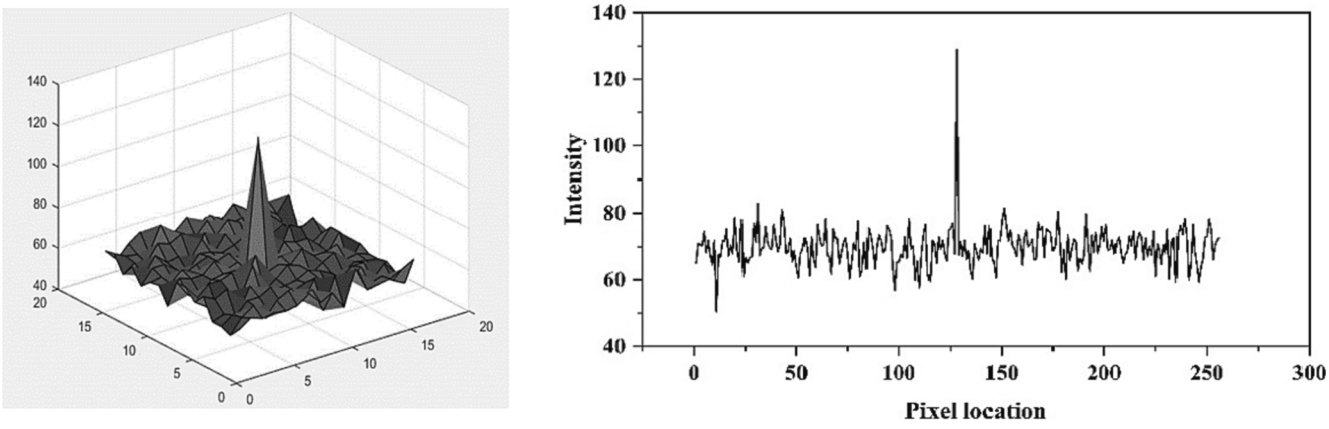

Fig. 1. the autocorrelation function of a 16 × 16 random coding array and the cyclic autocorrelation function of a one-dimensional random sequence.

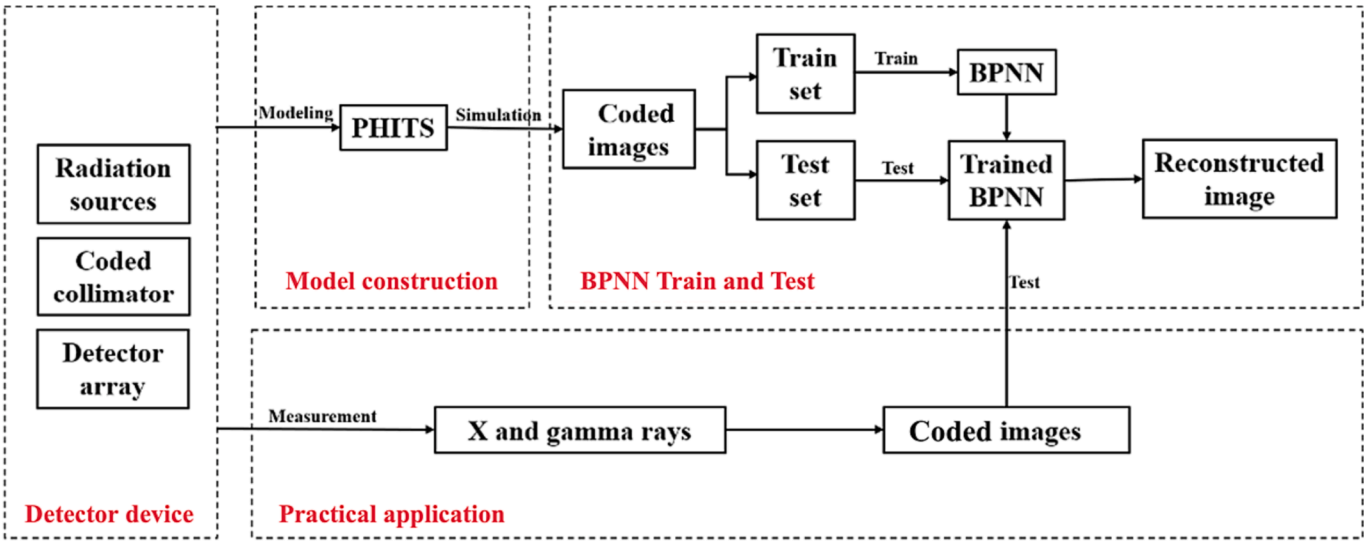

Fig. 2. Block diagram of the BPNN method for coded image reconstruction.

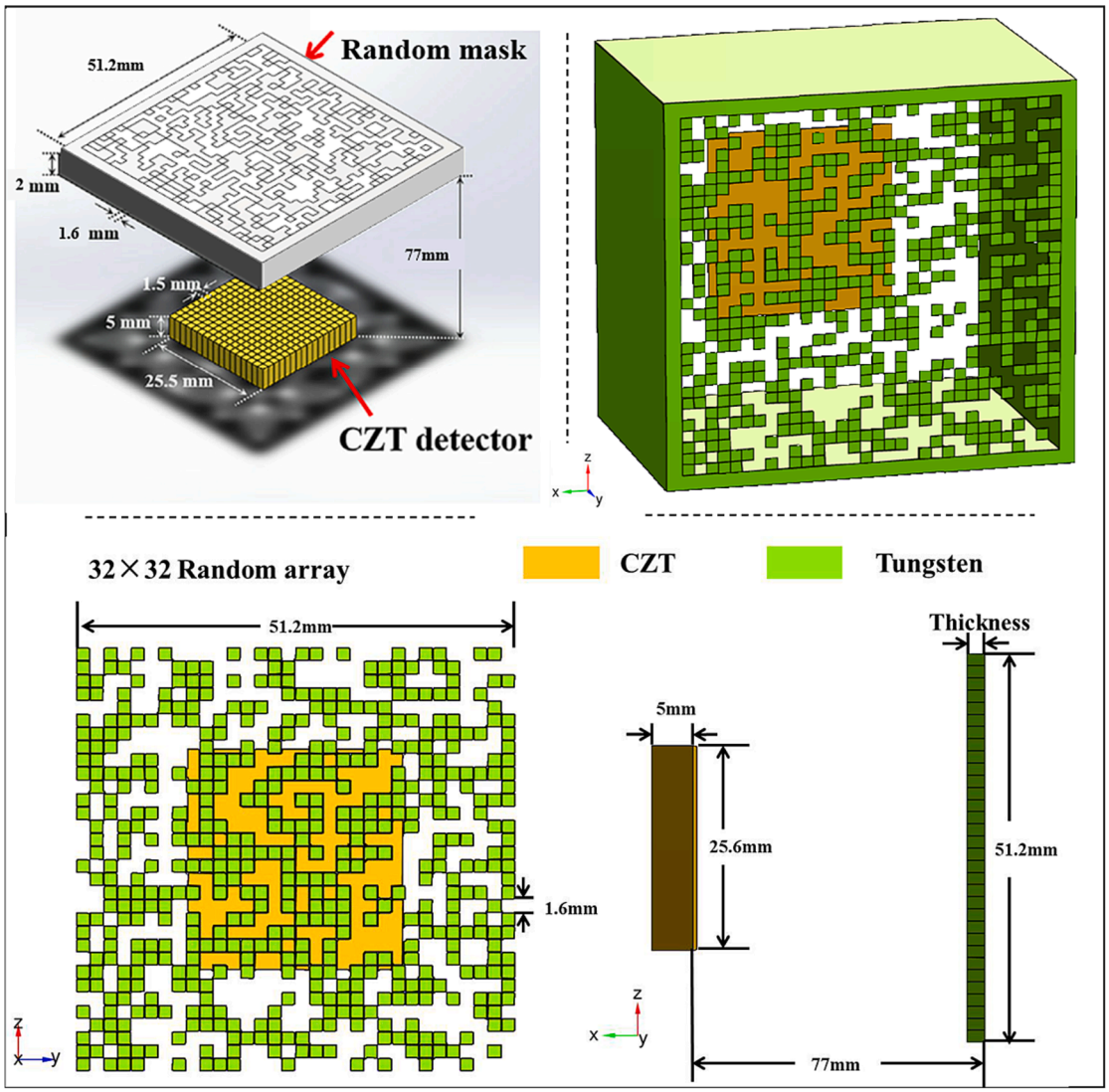

Fig. 3. Upper left: schematic of the coded mask and pixel detector. Upper right: Monte Carlo model in PHITS. Bottom: Specific parameters of the model in phits.

related operation reconstruction algorithms have become one of the commonly used technical approaches for spatial coding aperture imaging. The coding array of the mask was a random code of order 32 × 32 made of tungsten with a length of 51.2 mm. The size of the single hole was 1.6 mm × 1.6 mm, and the thickness of the mask was 2 mm, which can shield photons. The final Monte Carlo model is shown in Fig. 3, and the parallel distance of the mask and CZT detector was 77 mm. The parameters of the designed Randomly-coded-aperture gamma camera are shown in Table 1. In theory, it can achieve an FCFOV (Full Coded Field of View) of 20.24°×20.24° and a spatial resolution of 1.19°.

The PCFOV (Part Coded Field of View) was about 3.8 times that of the FCFOV. The area between the green box and the red box was the area where 1–50 % of the partially coded data was included in the reconstruction. This would make the FOV 2.8 times larger than the FCFOV. As can be seen in Fig. 4, within the 50 % of the PCFOV, the hot spot can be located more clearly. As the PCFOV was enlarged, the imaging effect degraded significantly. When the PCFOV was between 25 % and 50 %, which was the region between the blue box and the green box, the radioactive source image could not be reconstructed. Therefore, the follow-up research mainly focuses on the hot spot reconstruction of FCFOV.

3.2. Data acquisition and BPNN train

The training data were obtained by Monte Carlo simulation. In the simulation, a radioactive source was placed 1 m away from the mask, and the photons were approximately incident from one point to the mask. The region in the FOV of the gamma camera on the plane where the radioactive source was located was discretized into a 17 × 17 image, and a two-dimensional array reflecting the actual position of the radioactive source was obtained, where 1 indicated that the pixel had a radioactive source, and 0 indicated no radioactive source. The source image and coded image in each simulated imaging situation were considered a set of data samples; the source image was used as input data, and the coded image was considered output data. PHITS was used to simulate the imaging results when a single radiation source was located at 289 different locations, and then a large amount of training data was obtained in a short period of time through the superposition of single point source detection data. The simulation data accumulated over 60 s to reduce the influence of irrelevant noise data in the training data on the error convergence. The total number of training samples was one million; 90 % of the data was used for training, and the remaining data was used for testing. The optimized parameters of BPNN are shown as follows. The input data length of the BPNN network model (Fig. 5) constructed in this article was the detector data length, which is 256, and the output data length was the number of reconstructed image pixels, which is 289. The number of hidden layers is 1, and the number of hidden layer neurons is 300. The activation function was sigmoid. The dropout regularization strategy was used to reduce the over-fitting of the model. The loss function was the root mean square error.

3.3. Experimental device

The parameters of the experimental platform correspond to the Monte Carlo model settings, as shown in Fig. 6. Small squares of 1.6 × 1.6 × 2 mm^3 tungsten with 99 % purity were used to construct the code collimator by splicing. Three code collimators have been made with open rates of 50 %, 70 % and 90 %. The CZT pixel detector used in this study was the MPS256-B produced by the Imdetek Company, which was made of pixelated CZT crystal and preamplifier special integrated circuit. The configuration circuit of FPGA and ADC was built externally, which could simultaneously process 256 channels of data and output the corresponding two-dimensional data array containing “channel” and “count” information. These data were used to calculate the total count and the counting rate of detectors. All pixels of the detector were energy calibrated before use. Table 2 shows the detector parameters, which were consistent with the parameters in the Monte Carlo model. The Randomly-coded-aperture Imaging device composed of CZT detector and coded collimator was fixed on the optical platform, and the coded collimator was fine-tuned with an accuracy of 0.1 mm through the X, Y, and Z axis displacement platform. Thus, the coded collimator and the detector were formed in space correspondence.

Table 1
Theoretical parameters of cameras under 32 × 32 random array.

Pattern	FCFOV	Angular resolution
32 × 32 random array	20.24°×20.24°	1.19°

4. Results and discussion

4.1. Reconstruction results under different time and energy measurements

This experiment simulated the imaging situation caused by gamma rays of different energy incident on the end of the imaging device by placing different radioactive sources on a plane. Theoretically, in order to simulate more realistically, the gamma rays should be maintained as parallel as possible when they reach the detector. This approach can reduce the collimation effect in the coded-aperture radiography theory and better compare the reconstruction effects among different reconstruction methods. The distance from the source to the detector should be sufficiently far. However, excessively far source-detector distance reduced the flux on the surface of the detector. Thus, more time was consumed to reduce the influence of noise data on the CNR of the reconstructed image. In this experiment, the distance between the source plane and the detector plane was 1.1 m, and the imaging time was reduced on the basis of ensuring sufficient photon flux on the detector surface. The sources were Co-57 (7.98 × 10^5 Bq), Ba-133 (4.14 × 10^5 Bq), and Eu-152 (3.44 × 10^5 Bq). Fig. 7 shows the imaging results using three radioactive sources, each of which is placed in the center of the FOV. The imaging qualities of the BPNN and related operations were compared. The reconstructed data included background noise, and the counts produced in the detector were approximately 720–730 per minute.

Fig. 7 intuitively shows the excellent reconstruction performance of BPNN under different radioactive sources. On the contrary, the use of correlation reconstruction calculation could not obtain valuable images despite the longer detection time. In Fig. 7, due to the inherent background noise generated by the reconstruction based on random coding and correlation operation, the reconstruction based on correlation operations produced a fixed highlight area at the bottom right of the image.

In order to compare the imaging results of BPNN and correlation operation, the time-varying trend of the CNR of reconstructed images under different energy radioactive sources was drawn, as shown in Fig. 8. Here, the radioactive source was replaced by an X-ray tube and placed in the center of the FOV. The X-ray tube used in the experiment was KYW900A X-ray tube produced by Shanghai Keyway Electronics. The target material was tungsten metal, the maximum anode voltage was 60 kV, and the anode current range was 0–1 mA. The X-ray energy spectrum at 60 kV tube voltage was tested by the radiation detection system. According to its energy peak, the count in the 45–55 keV energy region was selected as the codeing data.

Fig. 8 shows that when the imaging time increases, the BPNN can generally yield a higher CNR with a short time in the reconstructed image, and as time increases, the CNR remains constant. The main difference between X-ray and gamma-ray reconstructions at different energies was that they had different “speeds” to achieve a stable optimal CNR. Fig. 8 also shows that under different incident rays along with measure the increment of time, their respective stable optimal CNR values are extremely close. This conclusion indicated that under different X-ray and gamma-ray energy, the reconstructed image can reach an optimal value in a short time, regardless of the X-ray and

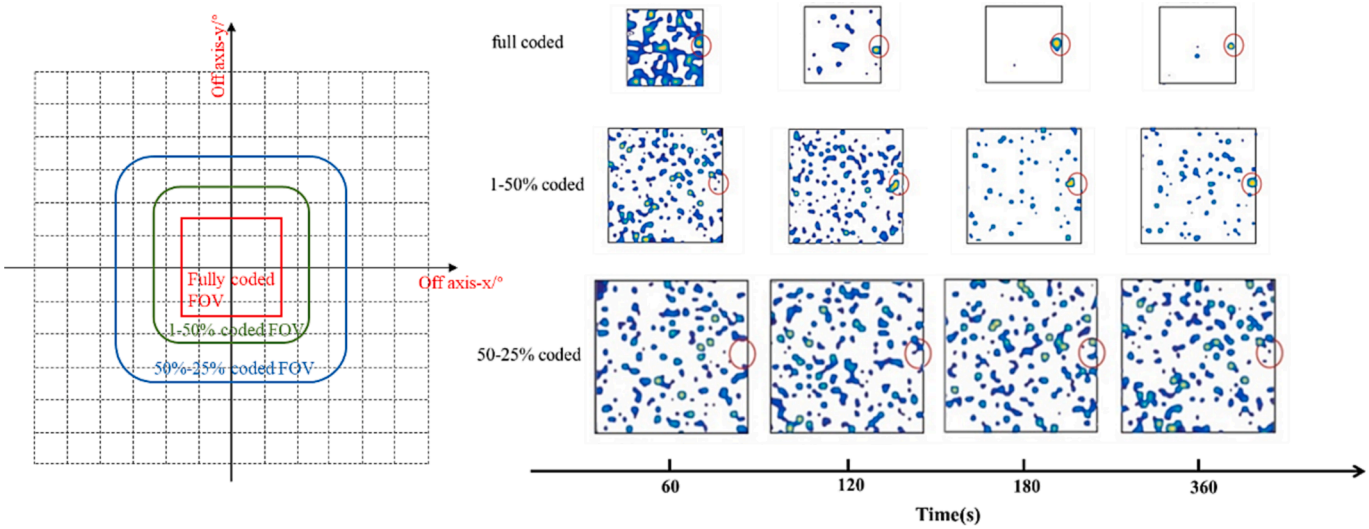

Fig. 4. Imaging effect of Co-57 source at the edge of FOV at different Partially Coded rates.

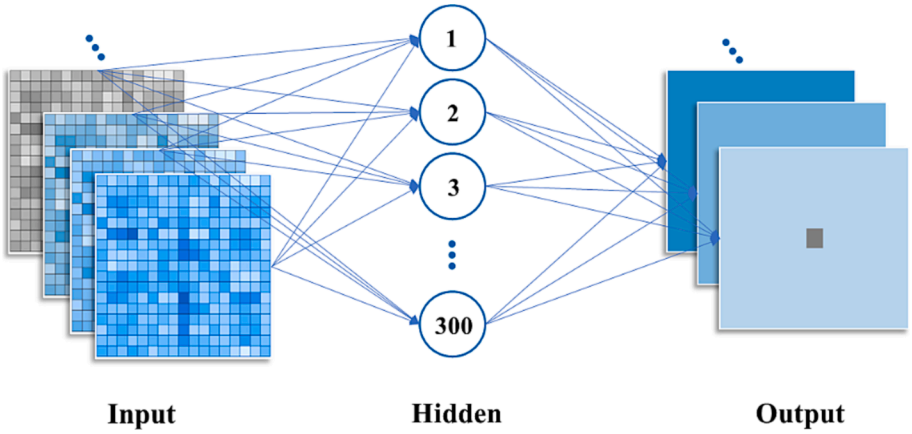

Fig. 5. Architectures of BPNN.

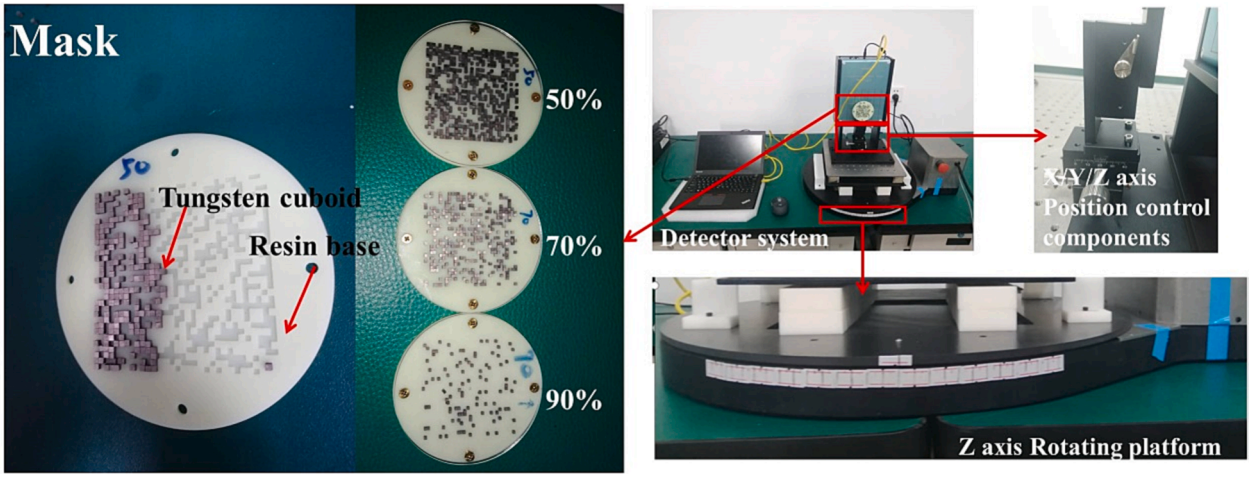

Fig. 6. Randomly-coded-aperture Imaging device experimental platform.

gamma-ray energy. The results show that the reconstruction method based on BPNN is different from the traditional correlation operation reconstruction. After detecting a certain number of effective photons, the image can obtain a stable and optimal CNR.

4.2. Effect of noise on the reconstructed image

In the experiment, no background shielding device was applied. The source was placed in the center of the camera's FOV, and the source term

Table 2
Specifications of the detector.

Features	Specifications
Material	CZT
Detector array	16 × 16
Voxel size	1.5 × 1.5 × 5 mm^3
Pixel pitch	1.6 mm
Detector size	25.4 × 25.4 × 5 mm^3
Energy range	20–700 keV

included all the rays generated by the X-ray tube. The source was 6 m away from the detector, and the detector count was approximately 900–1000 per minute. After calibrating the energy spectrum of CZT detector, the count with energy range of 45–55 keV was selected by adjusting the threshold value for image reconstruction to reduce the influence of noise term. Fig. 9 shows that the image quality has been improved to a certain extent after the noise is deducted. The data were selected when the imaging time was 32 min, the calculation shows that the CNR of the reconstructed image before denoising based on the BPNN reconstruction method is approximately 15 % lower than the CNR after deducting the noise, and the reconstruction based on correlation calculations is reduced by 65 %. The influence of noise on the correlation calculation is much greater than that of BPNN, thereby foreseeing the application of BPNN reconstruction method in a high background environment.

The reconstructed image after energy selection was selected when

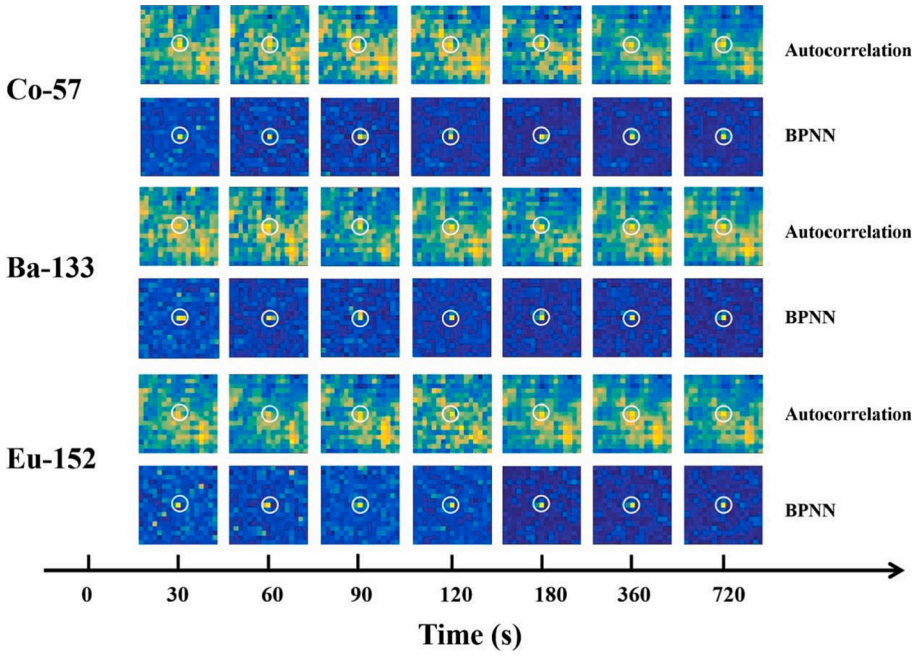

Fig. 7. Reconstruction renderings of different radioactive sources (Co-57, Ba-133, and Eu-152); the white circle is the accurate position of the source.

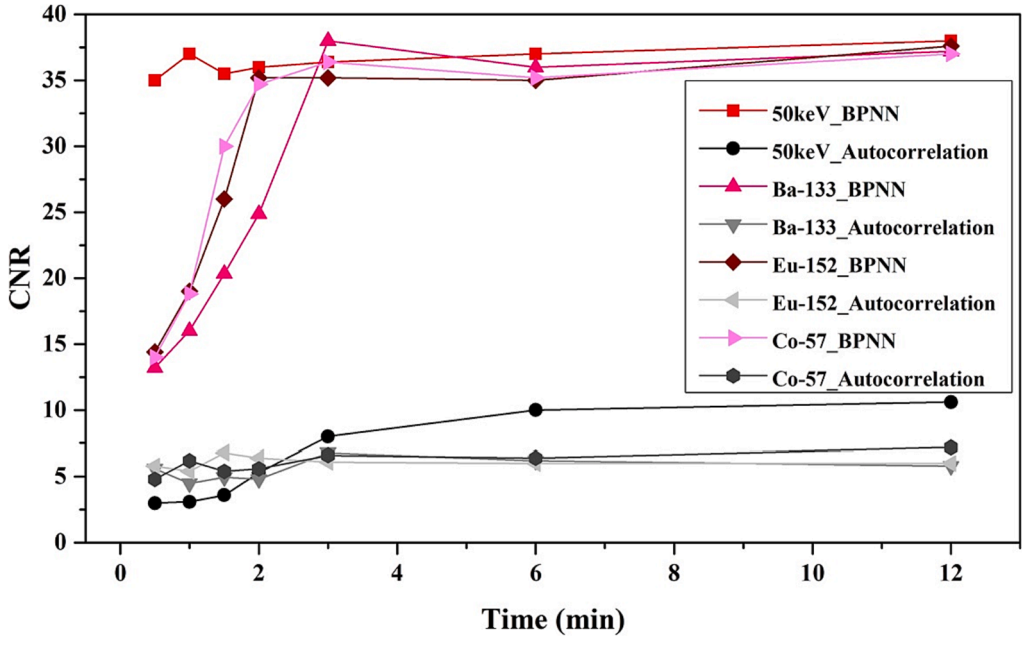

Fig. 8. Reconstructed image CNR changes with time.

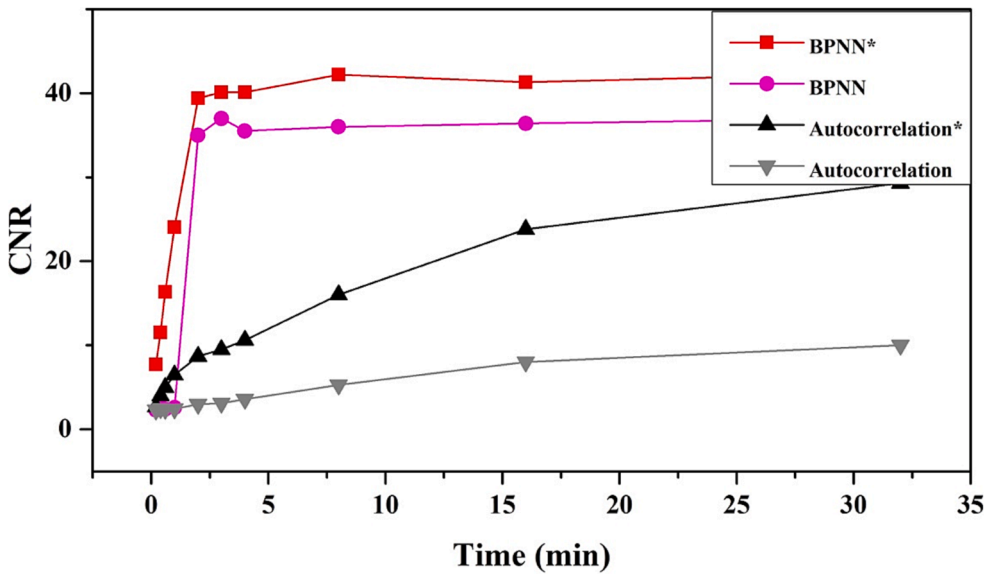

Fig. 9. The change trend of CNR of X-ray reconstruction image. (*: Select the count within the energy range of 45–55 keV).

the imaging time was 32 min, and the image matrix was rearranged into a one-dimensional array to analyze the excellent reconstruction performance of BPNN, as shown in Fig. 10. The ideal reconstruction method should contain two functions, as follows: the complete restoration of the characteristics of the coded signal and the suppression of signal-independent noise. The hidden layer in BPNN can increase the mapping ability of the network and enable it to solve nonlinear problems and multidimensional function approximation problems. Therefore, the use of BPNN with hidden layers is expected to simultaneously achieve code feature restoration and signal-independent noise suppression, as well as low-noise coded image reconstruction. Fig. 10 is the reconstructed intensity profile of the light source. BPNN reconstruction shows extremely low average background noise; thus, identifying hot spots in the reconstructed image in practical applications is easy. On the contrary, the average background noise of the reconstructed PSF obtained by the correlation operation is much larger than that of the BPNN. This finding proves that the reconstruction method based on the correlation operation is more susceptible to the fluctuation of the background noise.

4.3. *Influence of aperture ratio on imaging quality*

To further analyze the similarities and differences between BPNN decoding and traditional correlation operation decoding, different random coding aperture rates were set up to study the effect of aperture rate with BPNN decoding. In Table 3, the X-ray generated by the ray tube was used, the imaging time was 16 min, and the detector count was approximately 15,000 after the energy selection process. The peak pixel position of the reconstructed image is not at the theoretical position as an error reconstruction. Experiments show that the aperture ratio has a great influence on the reconstruction accuracy. This was due to the small difference between the reconstructed peak and the background mean value, and the background fluctuation was large. The image CNR of the reconstruction method based on BPNN also had a downward trend with the increase in the aperture rate. However, at an aperture rate of 90 %, the reconstructed image CNR and the reconstruction accuracy were

Table 3
Accuracy and CNR of the reconstructed image.

aperture rate	50 %	70 %	90 %
Rebuild accuracy of BPNN	88 %	80 %	75 %
Rebuild accuracy of Autocorrelation	43 %	26 %	8 %
CNR of BPNN	21	17.2	16.2
CNR of Autocorrelation	9.7	6.9	3.5

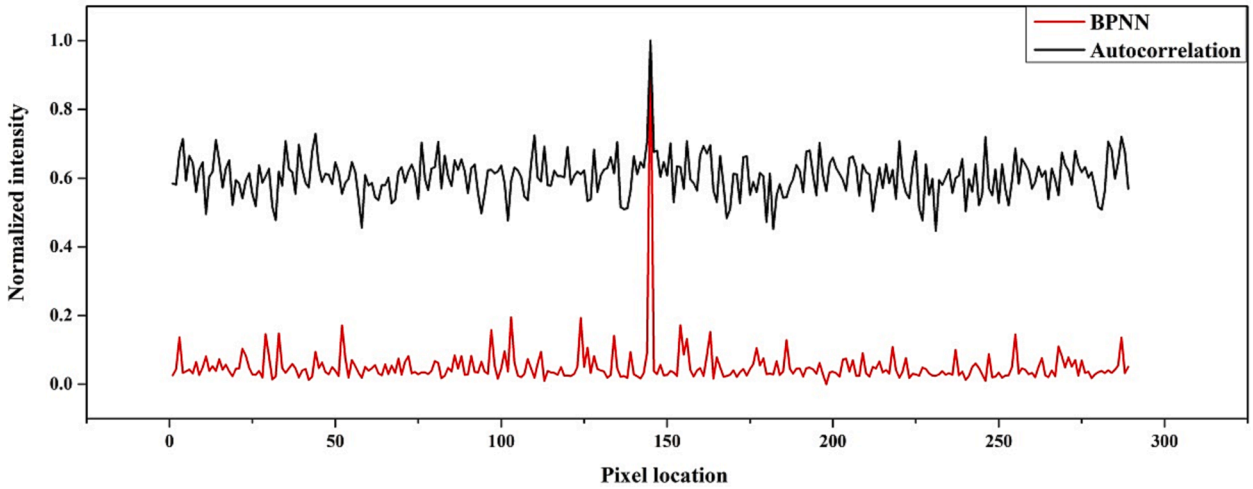

Fig. 10. Normalized 1D point spread function of reconstructed image.

always maintained at a high level. The production of code plates usually included high-density metal materials, such as tungsten. Increasing the opening rate has a certain implication in reducing the overall weight of the equipment.

4.4. Uniformity of imaging quality in the FOV

The ideal coded-aperture imaging theory requires that the thickness of the code plate is zero, and it has a 100 % shielding effect on incident photons of any energy.

In the actual situation, the code plate was not an ideal zero thickness. When the rays were incident from the edge of the FOV, the quality of the reconstruction at the edge of view would be reduced due to the collimation effect. The increase in the thickness of the collimator or the change in the FOV can exacerbate this effect. The imaging performance of the BPNN method was evaluated with X-ray, and 4.5 m distance from the detector with an imaging time of 10 s. The imaging FCFOV of the device was $20.24^\circ \times 20.24^\circ$. The connection between the center of the detector and the center of the encoder plate was set as the central axis, and the angle between the center and the edge was $-10.12^\circ \sim +10.12^\circ$ (Fig. 11).

Fig. 12 shows the variation of reconstructed image CNR with off-axis angle. The images obtained by the BPNN method can accurately distinguish the position of the source when the source was located at the center and edge of the FCFOV. The correlation calculation shows that the CNR of the reconstructed image decreases with the offset of the off-axis angle. In all positions, the CNR of the results of the BPNN method was higher than that of the correlation analysis method. Therefore, the reconstruction method of BPNN shows better uniformity of imaging quality in the FOV, as shown in Fig. 13.

4.5. Analysis of imaging performance of multi-point source

In the application of space radiation detection, in most cases, only the X-ray and gamma ray incident in one direction need to be positioned. At the same time, the X-ray and gamma ray incident in two or more directions within the detection field of vision are small probability events. However, in order to deal with this possible situation, we set Co-57 with activity of 7.98×10^5 in the imaging field of the experimental equipment for experimental imaging verification at a distance of 1 m. The radioactive source was placed at the off-axis angles of 0° and 10.12° as shown in Fig. 14(a) for 60 s coded data acquisition, and the double-point source data was obtained by any two overlaps of the coded data collected three times. Fig. 14(b) shows the reconstruction results of the two-point radioactive source by BPNN method, the ideal imaging result should be that the hot spot is located on the circled pixel. The background noise of the reconstructed image by BPNN method was small, and the position of the two-point source was recognized. There is no problem of complete reconstruction failure or wrong indication of the location of the radiation hot spot. When the radiation source is offset from the center, the imaging effect is relatively reduced. The reason for this phenomenon is that the obliquely incident photons produce repeated counts in several adjacent pixels of the detector, which blurs the encoded image, and results in the count of the neighboring pixels of the reconstructed image hotspots. The small FOV of gamma camera can be set to reduce this phenomenon. In the design of Randomly-coded-aperture Imaging device, the trade-off between detector thickness and photon diffusion should be considered in the design.

5. Conclusion

A BPNN-based reconstruction method for coded-aperture imaging was proposed to improve the quality of reconstructed images. A compact gamma camera with energy response range of 20 keV – 700 keV based on CZT pixel detector and random mask was constructed to study the effectiveness of the BPNN method in image reconstruction under various conditions. The simulation results showed that the trained BPNN can be used in the reconstruction process of coded images and can effectively reduce image noise. The CNR of the images obtained by the BPNN method was larger than that obtained by correlation analysis method. Therefore, this method can be used for real-time measurement and dynamic monitoring of space hard X-ray and gamma ray, and has great application potential in space detection and other fields. In addition, excellent spatial angular resolution is our main objective. We can use different sampling precisions or design the size and shape of code aperture to improve the spatial angular resolution and uniformity of the reconstructed image.

CRediT authorship contribution statement

Zeyu Wang: Conceptualization, Methodology, Formal analysis, Data curation, Writing – review & editing. **Chao Wang:** Conceptualization, Methodology, Formal analysis, Data curation, Writing – original draft. **Pin Gong:** Resources, Data curation, Supervision, Funding acquisition. **Liansheng Li:** Supervision, Funding acquisition. **Zhimeng Hu:** Supervision. **Yongqiang Shi:** Supervision. **Xiaolei Shen:** Validation, Formal analysis. **Cheng Zhou:** Supervision. **Xiaoxiang Zhu:** Supervision. **Xiaobin Tang:** Supervision, Funding acquisition.

Declaration of Competing Interest

The authors declare that they have no known competing financial interests or personal relationships that could have appeared to influence the work reported in this paper.

Data availability

The authors are unable or have chosen not to specify which data has

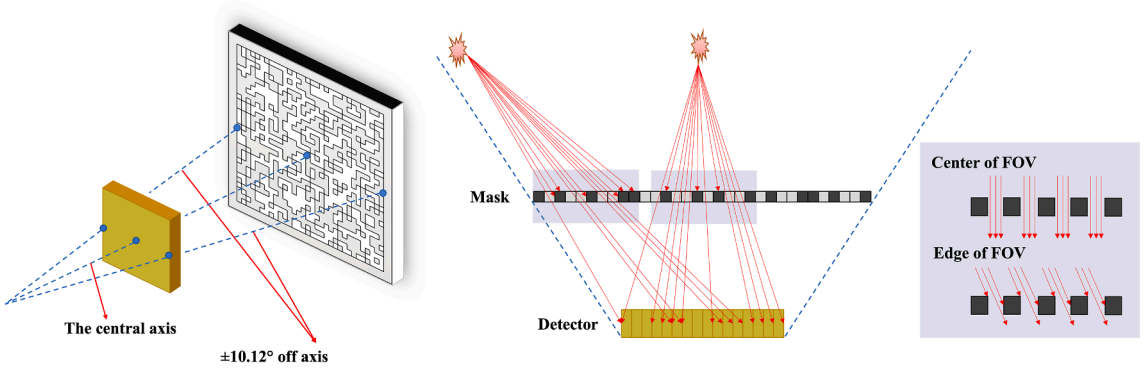

Fig. 11. Left: Schematic of the off-axis angle range of the entire device. Right: Transmission process of photon when rays are incident from the center and edge of the FOV.

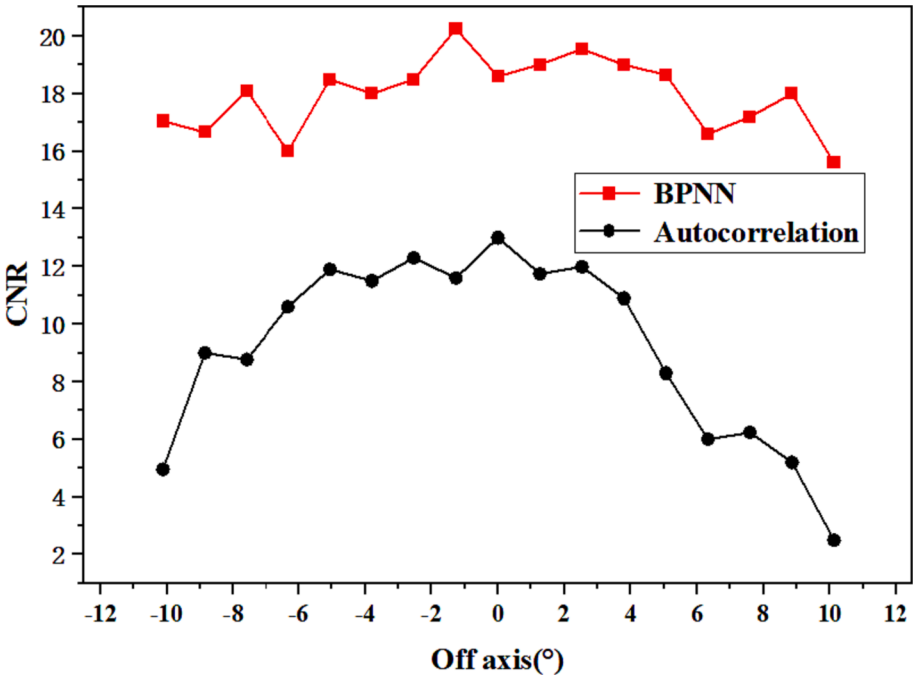

Fig. 12. Variation of reconstructed image CNR with off-axis angle.

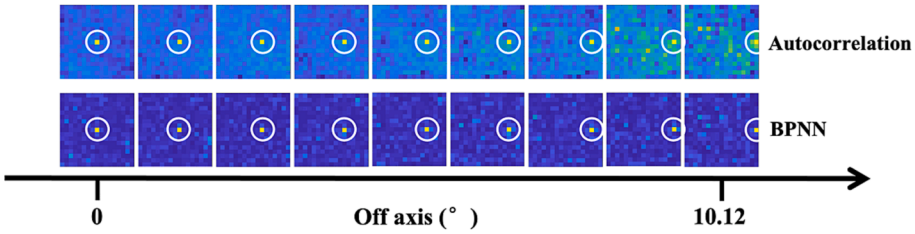

Fig. 13. Effect diagram of the reconstructed image changing with the off-axis angle.

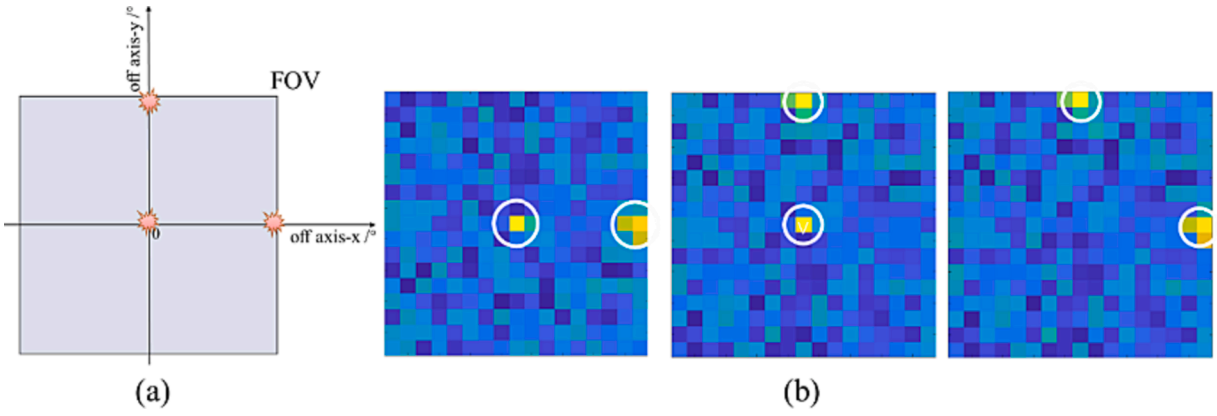

Fig. 14. Actual position of radioactive source (a) Imaging results of dual radioactive sources at different positions (b).

been used.

Acknowledgement

This work was supported by the State Key Laboratory of Intense Pulsed Radiation Simulation and Effect(Grant No. SKLIPR2023), the Lab of Space Optoelectronic Measurement & Perception(Grant No. Lab-SOMP-2020-03), the Primary Research and Development Plan of Jiangsu Province (Grant No. BE2022846), China Postdoctoral Science Foundation (Grant No. 2022M721659), and the Fundamental Research Funds for the Central Universities (Grant No. NC2022006, NG2023002).

References

Ballesteros, F.J., Muro, E.M., Luque, B., 2001. Speeding up image reconstruction methods in coded mask γ cameras using neural networks: application to the EM algorithm. Experimental Astronomy 11, 207–222. https://doi.org/10.1023/A:1013101111446.

Berrim, S., Lansiart, A., Moretti, J.L., 1996. Implementing of maximum likelihood in tomographical coded aperture. International Conference on Image Processing 745–748. https://doi.org/10.1109/ICIP.1996.561004.

Cenkeramaddi, L.R., Genov, G., Kohfeldt, A., Njøten, K., Rostad, M.E., Skogseide, Y., Roscoe, M., Solberg, A., Stadsnes, J., Ullaland, K., Østgaard, N., Budtzjørgensen, C., Kuvvetli, I., Mikkelsen, S., Maehlum, G., 2012. Low-energy CZT detector array for the ASIM mission. IEEE International Instrumentation and Measurement Technology Conference Proceedings 2012, 2119–2123. https://doi.org/10.1109/TNS.1996.4324349.

Cieślak, M.J., Gamage, K.A.A., Glover, R., 2016. Coded-aperture imaging systems: Past, present and future development–A review. Radiation Measurements 92, 59–71. https://doi.org/10.1016/j.radmeas.2016.08.002.

Ding, J., Noshad, M., Tarokh, V., 2016. Complementary lattice arrays for coded aperture imaging. Journal of the Optical Society of America A 33, 863–881. https://doi.org/10.1364/JOSAA.33.000863.

Fenimore, E.E., Cannon, T.M., 1978. Coded aperture imaging with uniformly redundant arrays. Applied Optics 17, 337–347. https://doi.org/10.1364/AO.17.000337.

Fitzgerald, J.G.M., Burggraf, L.W., Kowash, B.R., Hull, E.L., 2013. A modulating liquid collimator for coded aperture adaptive imaging of gamma-rays. IEEE Transactions on Nuclear Science 60, 2300–2307. https://doi.org/10.1109/TNS.2013.2259052.

Gottesman, S.R., Fenimore, E.E., 1989. New family of binary arrays for coded aperture imaging. Applied Optics 28, 4344–4352. https://doi.org/10.1364/AO.28.004344.

Grindlay, J., Hong, J., Allen, B., Barthelmy, S., Baker, R., 2011. Development of tiled imaging CZT detectors for sensitive wide-field hard X-ray surveys to EXIST. Nuclear Instruments & Methods in Physics Research 652, 671–673. https://doi.org/10.1016/j.nima.2010.09.160.

He, J., Tang, X., Gong, P., Wang, P., Han, Z., Yan, W., Gao, L., 2018. Spectrometry analysis based on approximation coefficients and deep belief networks. Nuclear Science and Techniques 05, 88–97. https://doi.org/10.1007/s41365-018-0402-4.

He, J., Tang, X., Gong, P., Wang, P., Wen, L., Huang, X., Han, Z., Yan, W., Gao, L., 2018. Rapid radionuclide identification algorithm based on the discrete cosine transform and BP neural network. Annals of Nuclear Energy 112, 1–8. https://doi.org/10.1016/j.anucene.2017.09.032.

Krimm, H.A., Holland, S.T., Corbet, R.H.D., Pearlman, A.B., Ukwatta, T.N., 2013. The swift/bat hard x-ray transient monitor. The Astrophysical Journal Supplement Series 38 (1), 882–887. https://doi.org/10.1088/0067-0049/209/1/14.

Macwilliams, F.J., Sloane, N.J.A., 1977. Pseudo-random sequences and arrays. Proceedings of the IEEE 64, 1715–1729. https://doi.org/10.1109/PROC.1976.10411.

Martineau, A., Rocchisani, J.M., Moretti, J.L., 2010. Coded aperture optimization using Monte Carlo simulations. Nuclear Instruments and Methods in Physics Research A 616, 75–80. https://doi.org/10.1016/j.nima.2010.02.261.

McCleskey, M., Kaye, W., Mackin, D.S., Beddar, S., He, Z., Polf, J.C., 2015. Evaluation of a multistage CdZnTe Compton camera for prompt γ imaging for proton therapy. Nuclear Instruments and Methods in Physics Research Section A Accelerators Spectrometers Detectors and Associated Equipment 785, 163–169. https://doi.org/10.1016/j.nima.2015.02.030.

Olmos, P., Diaz, J.C., Perez, J.M., Garcia-Belmonte, G., Gomez, P., Rodellar, V., 1992. Application of neural network techniques in gamma spectroscopy. Nuclear Instruments and Methods in Physics Research Section a: Accelerators, Spectrometers, Detectors and Associated Equipment 312, 167–173. https://doi.org/10.1016/0168-9002(92)90148-W.

Phillips, K.J.H., Feldman, U., Land, E., 2008. Ultraviolet and X-ray Spectroscopy of the Solar Atmosphere: Plasma diagnostic techniques. Cambridge University Press. https://doi.org/10.1017/CBO9780511585968.

Shen, X.L., Gong, P., Tang, X.B., 2020. Encoding methods matching the 16×16 pixel CZT detector of a coded aperture gamma camera. Nuclear Science and Techniques 31, 84–91. https://doi.org/10.1007/s41365-020-00796-5.

Sihver, L., Mancusi, D., Sato, T., Niita, K., Iwase, H., Iwamoto, Y., Matsuda, N., Nakashima, H., Sakamoto, Y., 2007. Recent developments and benchmarking of the PHITS code. Advances in Space Research 40, 1320–1331. https://doi.org/10.1016/j.asr.2007.02.056.

Zhang, R., Gong, P., Tang, X.B., 2019. Reconstruction method for gamma-ray coded-aperture imaging based on convolutional neural network. Nuclear Instruments and Methods in Physics Research A 934, 41–51. https://doi.org/10.1016/j.nima.2019.04.055.